REPORT NO.
UCB/SEMM-1999/10

STRUCTURAL ENGINEERING
MECHANICS AND MATERIALS

TOWARD AN UNDERSTANDING OF THE OBSERVED BUCKLING MODES OF REINFORCING BARS IN CONCRETE COLUMNS

BY

W. M. FALK

AND

S. GOVINDJEE

SEPTEMBER 1999

DEPARTMENT OF CIVIL AND ENVIRONMENTAL ENGINEERING
UNIVERSITY OF CALIFORNIA
BERKELEY, CALIFORNIA

Toward an Understanding of the Observed Buckling Modes of Reinforcing Bars in Concrete Columns

W. M. Falk* and S. Govindjee†

September 27, 1999

Abstract

The buckling and post-buckling behavior of reinforcing bars in spirally reinforced columns is studied using finite deformation kinematics and a linear elastic constitutive law. Analytical results show the initially straight elastic system to buckle first in a single spacing mode and then make a "snap" transition to a multiple spacing mode similar to that observed in the actual system. The results are verified using a more general elastic finite element solution.

Introduction

The plastic hinge region at the base of concrete columns is arguably the most vital detail in the vocabulary of structural engineering. The buckling of reinforcing bars within this region has been observed in earthquake damaged buildings and in the laboratory, however, the mechanisms that govern this behavior are poorly understood.

The study of reinforcement buckling holds technical challenges because it combines the nonlinearities of material, geometry and contact. Bresler and Gilbert [1] initiated the study of the phenomenon in 1961. The model they proposed has served as the benchmark for all of the models that have followed. This model is composed of an initially straight bar which is allowed to deflect in one direction in an assumed sinusoidal shape. The deflecting bar must overcome equally spaced springs which represent the restraining action of the transverse reinforcement. The kinematic assumption of small deformation is made which is consistent only when considering deformed configurations arbitrarily close to the straight configuration. The tangent stiffness method is used to determine the spacing of transverse reinforcement that is needed to keep the bar from buckling before it yields.

Subsequently, many other writers have proposed models with improved constitutive laws [4], [9] and more general solutions using finite elements [4] and eigensolutions [6]. Some of the models show agreement with experiments on a single bar [4] and other models have been calibrated using experimental results for use in design [5]. None of the models have been able to adequately explain the observed buckling mode.

In this paper we seek to explain the observed buckling mode and demonstrate its evolution analytically. Since observation of the buckled bar can be made only after the bar protrudes from the concrete, the formulation must be accurate for finite deformations. The consideration of finite deformations makes solution of equilibrium equations more difficult. To keep the problem relatively simple, only elastic constitutive laws have been used for the longitudinal bars. Admittedly, this is not repre-

*Former Graduate Student, Department of Civil Engineering, University of California, Berkeley. Currently Graduate Student, Department of Aerospace Engineering and Mechanics, University of Minnesota.

†Associate Professor, Department of Civil Engineering, University of California, Berkeley.

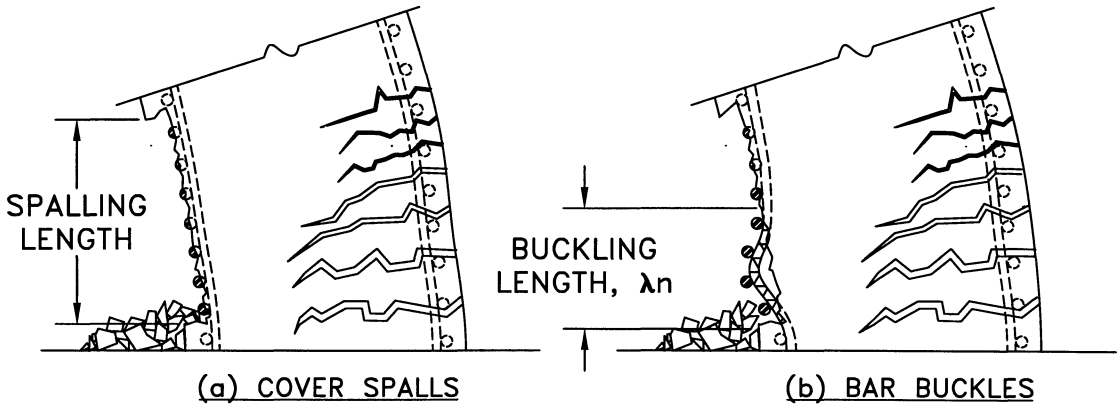

Figure 1: Observed phenomenon

sentative of actual reinforcing bars, however, the results are of value nonetheless. The focus here is strictly qualitative—in studying the elastic system in finite deformation, much can be learned about the actual one.

A second novel aspect of this research is the treatment of the spiral reinforcement. Before the buckling of longitudinal bars, spiral reinforcement is often strained beyond its yield point. In order to properly model this a rigid–plastic model is adopted for the spiral material. In addition, the kinematics of the spiral as it is pushed away from the core are modeled in a more representative manner than has been attempted before.

Observed Phenomenon

In the most common laboratory test for earthquake resisting columns the following loadings are applied: (1) The column is loaded with a constant axial load to represent gravity. (2) In order to simulate the action of an earthquake, the column is deformed side-to-side by the action of lateral forces. The hinge zone experiences the following sequence of observable events:

1. The cover spalls to a height of 2–3 column diameters before the longitudinal bar buckling is observed. (Figure 1a)

2. The buckled bar emerges from the concrete, the buckle is observed to have a length from 3–6 spiral spacings. The buckled bar exerts great force on the spiral, often causing a loss of confinement (Figure 1b).

The nature of the phenomenon is that two states of deformation are known: the initial state and a finitely deformed state. The initial state is observed when the column is constructed. It is seen that a straight bar is installed. Next, the bar is observed in a buckled configuration as it emerges from the concrete cover. The buckling is seen to occur over multiple spiral spacings but not over the entire spalling length.

Since the intermediate levels of deformation are hidden, the objective is to explain how the deformed state is reached from the initial state. To make matters interesting, the deformation observed cannot be "scaled-up" from a small deformation theory. It will be shown analytically that the buckling must initiate over a single spacing. However, when finite levels of deformation are taken into account, the buckling mode can make a transition from the sin-

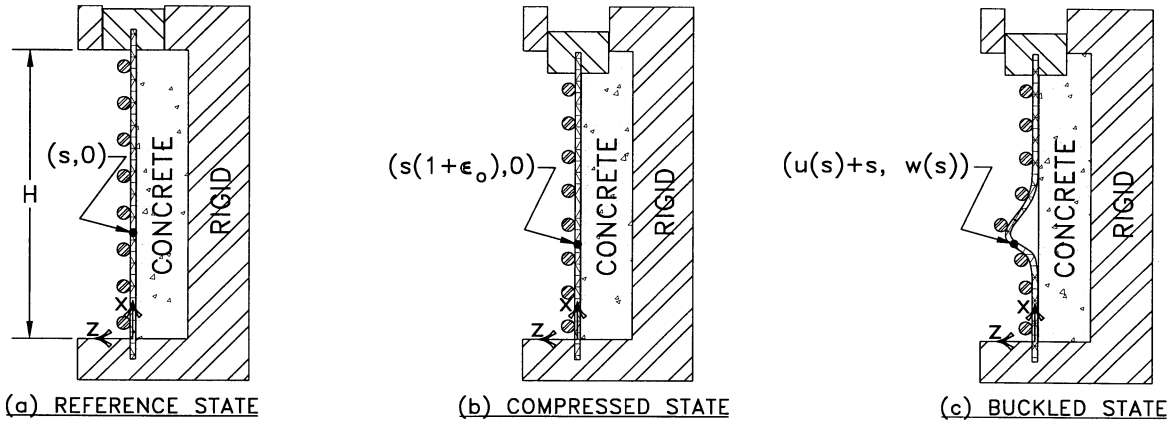

Figure 2: States of deformation

gle spacing mode to a multiple spacing mode similar to that observed in the laboratory.

Model Description

Consider a simplified model of one longitudinal bar. The bar contacts the core over a continuous interval on one side and contacts the spiral at discrete points on the other side. The spiral spacing is λ. The contact surfaces convey only normal tractions to the bar. When the bar is straight, its axis is aligned with the x-axis. When the bar is deformed, it is assumed to deform only in the x, z plane.

Three equilibrium states are shown in Figure 2. In the remainder of this work they will be referred to as defined below.

Reference State – This is the unstressed configuration. The bar is straight with length, H.

Compressed State – The straight bar compressed uniformly with infinitesimal axial strain, ϵ_o. There is no transverse displacement.

Buckled State – The bar with a buckle of arbitrary shape.

Material and Spatial Coordinates

Consider again Figure 2. Let S be the set of material points lying on the centerline of the bar. The points are identified by their x-coordinate in the reference state so that $S = [0, H]$.

Consider a point $s \in S$ as the bar deforms. In the compressed state, the bar is uniformly compressed with infinitesimal axial strain ϵ_o, so s lies on the x-axis with spatial coordinates $\{x(s), z(s)\} = \{s(1 + \epsilon_o), 0\}$.

In the buckled state, the point will be moved an amount $u(s)$ in the x-direction and an amount $w(s)$ in the z-direction. So that the spatial coordinates will be $\{x(s), z(s)\} = \{s + u(s), w(s)\}$.

Potential Energy

There are three separate force systems acting on the bar. Each is derived from its own potential energy function. The three potential energy functions are: (1) the potential of the axial load, U_{load}; (2) the potential of the strain energy, U_{strain}; and (3) the potential of the spiral, U_{spiral}. The potential energy of the system can be written as the sum of these terms,

$$U = U_{load} + U_{strain} + U_{spiral}\,. \qquad (1)$$

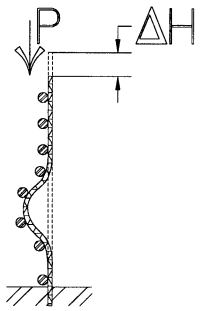

Figure 3: Potential energy of axial load

In the following sections, the terms of the potential energy equation are shown to be functionals of the centerline deformations, $u(s)$ and $w(s)$. Therefore, each term of the potential energy equation will be quantifiable for any deformation $u(s)$ and $w(s)$. The three potential functionals will be denoted with a superscript carrot, $\hat{(\cdot)}$.

Axial Load Potential, U_{load}

By assumption the axial load, P, does not depend on the deformation – it is an externally applied force of constant magnitude. Therefore, if P moves downward through a distance ΔH (Figure 3) the change of potential is $-P\,\Delta H$. Where both P and ΔH are positive quantities. Identifying the reference state with $U_{load} = 0$, write

$$U_{load} = -P\,\Delta H\,. \tag{2}$$

The quantity ΔH is the amount by which the two ends of the bar approach each other,

$$\Delta H = -\int_0^H u'(s)ds = \Delta\hat{H}\left[u'(s)\right]\,. \tag{3}$$

Combining this with (2), we can write the axial load, U_{load}, as a functional of the displacement:

$$U_{load} = -P\;\Delta\hat{H}\left[u'(s)\right]\,. \tag{4}$$

Strain Energy of the Bar, U_{strain}

Reinforcing bars of typical dimensions buckle in the plastic range of material response. In order to analytically proceed we set aside this material non–linearity, and consider only the kinematic non–linearity of large deformation. In order to do this, a reinforcing bar of typical dimensions cannot be considered. Instead, consider a more slender bar made of a very high strength steel. As a result the new bar buckles elastically.

The assumption is made that the state of stress in the bar is a linear function of only the state of strain. Working with the Green–St.Venant strain tensor denoted, $\mathbf{E}$, and the Second Piola–Kirchhoff stress tensor denoted, $\mathbf{S}$. The relation between them is written using the fourth rank tensor, $\mathbf{C}$.

$$\mathbf{S} = \mathbf{C}\cdot\mathbf{E} \qquad \mathbf{C}\text{, a matrix of constants}$$

The strain energy stored in deforming a body, B, can be written

$$\begin{aligned} U_{strain} &= \frac{1}{2}\iiint_B \mathbf{S}\cdot\mathbf{E}\,dV \\ &= \frac{1}{2}\iiint_B (\mathbf{C}\cdot\mathbf{E})\cdot\mathbf{E}\,dV\,. \end{aligned} \tag{5}$$

The bar is assumed to be an Euler-Bernoulli beam. Based on the kinematic assumptions of the theory, the only non-vanishing strain component is E_{xx}, see [3] or [10]. Thus equation (5) reduces to

$$U_{strain} = \frac{1}{2}\iiint_B C_{xx}\,E_{xx}^2\,dV\,. \tag{6}$$

C_{xx} is the constant relating E_{xx} and its work conjugate S_{xx}. Imposing the usual assumption that allows an Euler-Bernoulli beam to satisfy zero–traction boundary conditions along its length, $S_{yy} = S_{zz} = 0$. The resulting state of plane stress identifies C_{xx} with the uniaxial elastic modulus, E.

$$U_{strain} = \frac{1}{2}\,E\iiint_B E_{xx}^2\,dV \tag{7}$$

E_{xx} is expressed as a function of the displacements $u'(s)$, $u''(s)$, $w'(s)$ and $w''(s)$. See [3] or [10] for the derivation.

$$E_{xx} = \frac{1}{2}\left[(1+u'(s))^2 + w'^2(s) - 1\right] - z\,\frac{w''(s)[1+u'(s)] - w'(s)\,u''(s)}{\sqrt{[1+u'(s)]^2 + w'^2(s)}} + \frac{1}{2}z^2\left[\frac{w''(s)[1+u'(s)] - w'(s)\,u''(s)}{[1+u'(s)]^2 + w'^2(s)}\right]^2, \quad (8)$$

where z is the material coordinate of the bar through its thickness. This dependency integrates into the section properties, and does not appear when U_{strain} is evaluated in equation (7). Therefore, we can write U_{strain} as a functional of the functions $u'(s)$ and $w'(s)$ and their derivatives,

$$U_{strain} = \hat{U}_{strain}[u'(s), u''(s), w'(s), w''(s)]\,. \quad (9)$$

Spiral Energy, U_{spiral}

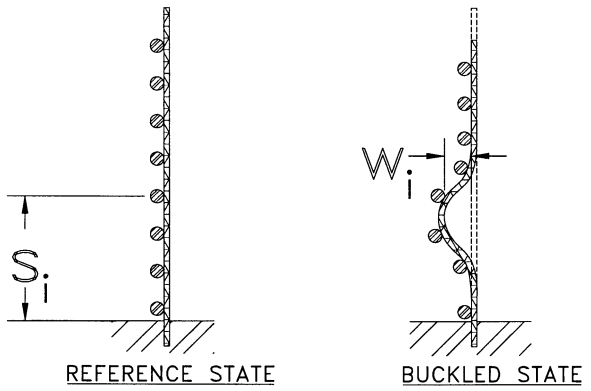

Figure 4: Configuration of spiral

Say we have m spirals turns over the length of our bar. Let s_i be the coordinate of the ith spiral turn in the reference state. As the bar deforms with transverse displacement $w(s)$, each spiral turn displaces an amount w_i (Figure 4), where:

$$w_i = w(s_i) \qquad i = \{1, 2, \ldots, m\} \quad (10)$$

Let the amount of potential energy stored in deforming one spiral turn be $U_{one\ spiral}(w_i)$. Then the potential energy stored in deforming the entire spiral:

$$U_{spiral} = \sum_{i=1}^{m} U_{one\ spiral}(w_i)\,. \quad (11)$$

In order to determine $U_{one\ spiral}$ as a function of the displacement w_i, the kinematics and equilibrium of the system are investigated. Consider the concrete column under load. As a concrete column compresses, its cross-section dilates; i.e. Poisson Effect. For a spirally reinforced column, the dilation has the effect of tensioning the spiral. This tension can be sufficiently high to yield the spiral. The Deformation Theory of Plasticity will be employed to consider this behavior [10]. For monotonic deformations we can "replace" the mechanical work done in deforming a plastic material by a strain energy. Thereby, a plastic material is treated as a non–linear elastic material.

Assume that immediately before the onset of buckling, the column has dilated from its original radius, R_o, an amount ΔR to have a radius R. As a result, the spiral goes from its unstressed state to having a uniform tension, T. (Figure 5) We will consider the spiral to be rigid-perfectly-plastic so that T will be the yield force for the spiral, $T = A_{spiral}F_y$, and will not be a function of the displacement. [1]

Consider what happens at the onset of buckling (Figure 6). When the bar moves away from the core a distance, w_i, it exerts a force on the spiral. We make the assumption that as the bar buckles, it moves monotonically away from the core at all points along its length. Based on this assumption we can identify the work done by the bar on the spiral, W_T, with a gain of potential of the spiral.

$$U_{one\ spiral}(w_i) = W_T(w_i) \quad (12)$$

The displacement w_i, increases the circumference of the spiral an amount $\Delta C(w_i)$ through

[1] This assumption is not required. The spiral could be modeled as elasto-plastic without affecting the nature of the final result. However, in the interest of simplicity, this model is used.

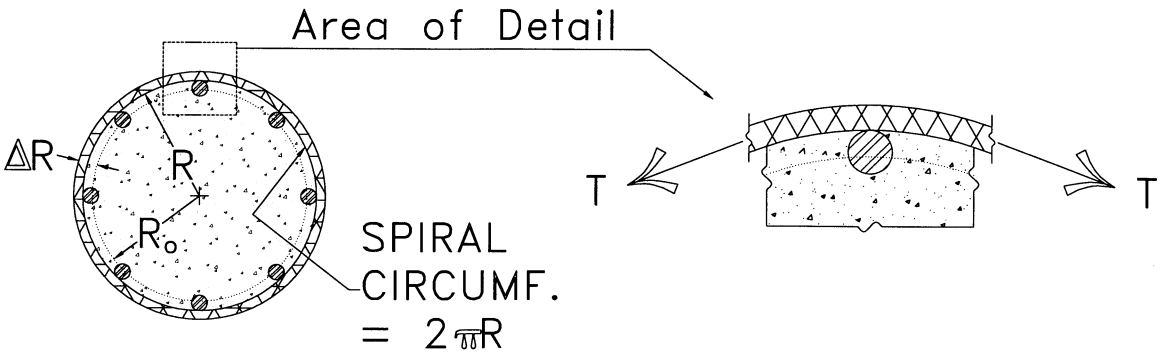

Figure 5: Cross section before buckling

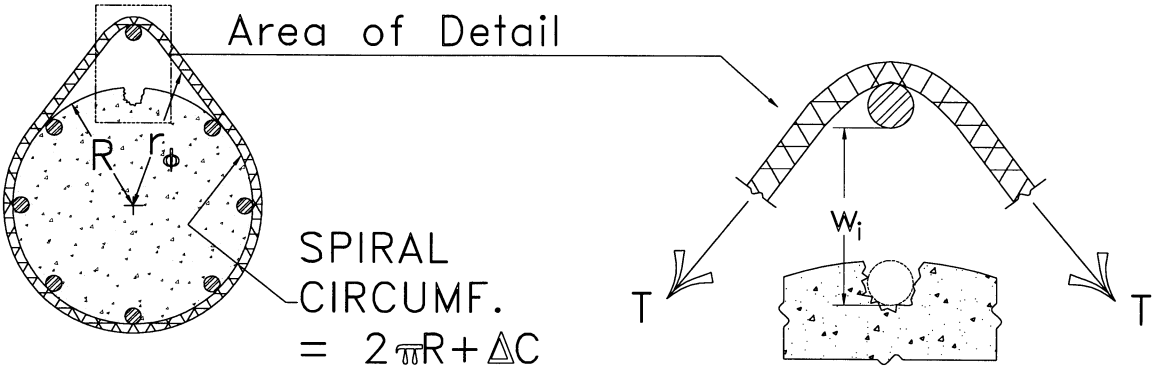

Figure 6: Cross section after buckling

the constant force, T. Therefore the work done by the bar on the spiral is

$$W_T(w_i) = T\ \Delta C(w_i)\,.$$

Combining this with (12) yields

$$U_{one\ spiral}(w_i) = T\ \Delta C(w_i)\,.$$

Putting this together with equation (11) gives

$$U_{spiral} = T \sum_{i=1}^{m} \Delta C(w_i)\,. \qquad (13)$$

Now the function $\Delta C(w_i)$ will be approximated by assuming the deformed shape of the spiral, $r_\phi(w_i)$ (Figure 6b):

$$r_\phi(w_i) = R + w_i \left(\frac{2\,\phi}{\pi}\right)^2 \qquad \phi \in [0, \frac{\pi}{2}]$$

The change in circumference as a function of w_i becomes

$$\Delta C(w_i) = 2\int_0^{\frac{\pi}{2}} \sqrt{r_\phi^2(w_i) + \left[\frac{\partial}{\partial\phi} r_\phi(w_i)\right]^2}\, d\phi - \pi R$$

$$= 2\int_0^{\frac{\pi}{2}} \sqrt{\left[R + w_i \left(\frac{2\phi}{\pi}\right)^2\right]^2 + \frac{64\, w_i^2\, \phi^2}{\pi^4}}\, d\phi - \pi R. \qquad (14)$$

Taken together, equations (10), (13) and (14) give us the ability to write the energy employed in deforming the spiral as a functional of the transverse displacement.

$$U_{spiral} = \hat{U}_{spiral}\,[w(s)] \qquad (15)$$

Equilibrium Based on Variation of One Parameter

The *Principal of Minimum Potential Energy* is used to consider the equilibrium of the buckled configuration characterized by the deformation functions $u(s)$ and $w(s)$. The Principle of Minimum Potential Energy states that *among all the configurations satisfying the prescribed geometric constraints, the state of equilibrium causes the potential energy to be stationary* [10]. This is written

$$\delta U = 0\,. \tag{16}$$

The *variation of the potential energy*, δU, is the change in the potential energy, U, when an infinitesimal displacement is imposed that satisfies the prescribed geometric constraints. This infinitesimal displacement is known as an *admissible variation*, denoted

$$[u(s), w(s)] \rightarrow [u(s) + \delta u(s), w(s) + \delta w(s)]\ .$$

Equation (16) describes an exact statement of equilibrium. However, in order to solve for the exact solution we must consider all the possible admissible deformations. For complicated systems this is generally not practicable. The best that can be done is an approximation of the deformation.

We proceed by guessing a form of the displacement that can be characterized by finitely many parameters. Then we vary the parameters infinitesimally in the potential energy functional. In this approximate form, The Principle of Stationary Potential Energy defines equilibrium states as a set of parameters for which infinitesimal variations cause no change in the potential energy.

Taking the simplest case, we consider variations in <u>one</u> deformation parameter, the amplitude, α. We define an equilibrium state as a state for which the potential energy, U, is stationary for infinitesimal changes, $\alpha \rightarrow \alpha + \delta\alpha$. For this, the variation of the potential energy

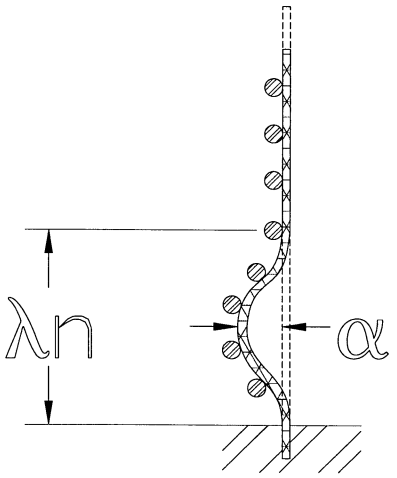

Figure 7: Assumed deformation

becomes the differential, [2]

$$\delta U = \delta\alpha\ \frac{\partial}{\partial\alpha} U = 0\,.$$

Since $\delta\alpha \neq 0$ we get a 1-dimensional equilibrium equation which is simply a partial derivative of the potential energy with respect to α,

$$\frac{\partial}{\partial\alpha} U = 0\,. \tag{17}$$

In the rest of this section, this equilibrium equation will allow us to determine the axial load, P, that when applied to the system equilibrates a buckle of amplitude, α.

Assumed Deformation

We assume that for any buckling length, n, the deformation of the bar can be parameterized by the amplitude of the buckle, α. (Figure 7) In order to do this, the lateral displacement is assumed sinusoidal over the buckled length and zero everywhere else.

$$w(\alpha, n, s) = \begin{cases} \alpha\left(\frac{1}{2} - \frac{1}{2}\cos\frac{2\pi s}{\lambda n}\right) & \text{if } s < \lambda n \\ 0 & \text{otherwise} \end{cases} \tag{18}$$

[2] This is the linear part, terms of higher order in $\delta\alpha$ are neglected since $\delta\alpha$ is infinitesimal regardless of the size of α.

Taking the derivative with respect to s, we get $w'(s)$ and $w''(s)$.

$$w'(\alpha,n,s) = \begin{cases} \alpha\frac{\pi}{\lambda n}\sin\frac{2\pi s}{\lambda n} & \text{if } s < \lambda n \\ 0 & \text{otherwise} \end{cases} \quad (19)$$

$$w''(\alpha,n,s) = \begin{cases} \frac{2\alpha\pi^2}{(\lambda n)^2}\cos\frac{2\pi s}{\lambda n} & \text{if } s < \lambda n \\ 0 & \text{otherwise} \end{cases} \quad (20)$$

In order to make the potential energy a function of α and n, we will need to make u' and u'' functions of α and n. To do this, we assume that the arc length does not change between the compressed state and the buckled state [3]

$$1+\epsilon_o = \sqrt{[1+u'(s)]^2 + w'^2(\alpha,n,s)}\,. \quad (21)$$

Recall that ϵ_o is the infinitesimal axial strain in the straight compressed bar,

$$\epsilon_o = -\frac{P}{E\,A_{bar}}.$$

Where A_{bar} is the cross-sectional area of bar. Solving (21) for u' as a function of ϵ_o, α, n and s,

$$u'(\epsilon_o,\alpha,n,s) = \sqrt{(1+\epsilon_o)^2 - w'^2(\alpha,n,s)} - 1\,. \quad (22)$$

Taking the derivative with respect to s gives

$$u''(\epsilon_o,\alpha,n,s) = -\frac{w'(\alpha,n,s)\;w''(\alpha,n,s)}{\sqrt{(1+\epsilon_o)^2 - w'^2(\alpha,n,s)}}\,. \quad (23)$$

The deformations (18), (19), (20), (22) and (23) are used to evaluate the functionals (4), (9) and (15). In this way, the functionals become *functions* of ϵ_o, α, n and s. These functions will be denoted with a superscript tilde, ($\tilde{\cdot}$):

$$\left.\begin{aligned} U_{load} &= -P\;\Delta\hat{H}\,[u'(s)]\circ u'(\epsilon_o,\alpha,n,s) \\ &= -P\;\Delta\tilde{H}(\epsilon_o,\alpha,n) \\ U_{strain} &= \hat{U}_{strain}[u'(s),u''(s),w'(s),w''(s)] \\ &\quad\circ\{u'(\epsilon_o,\alpha,n,s),u''(\epsilon_o,\alpha,n,s), \\ &\qquad w'(\alpha,n,s),w''(\alpha,n,s)\} \\ &= \tilde{U}_{strain}(\epsilon_o,\alpha,n) \\ U_{spiral} &= \hat{U}_{spiral}\,[w(s)]\circ w(\alpha,n,s) \\ &= \tilde{U}_{spiral}(\alpha,n) \end{aligned}\right\} (24)$$

Initial Buckling

In this section it will be shown that the buckle will always begin over one spacing. In order to do this all of the terms of the equilibrium are evaluated for a deformation where ϵ_o and α are assumed small.

$$|\epsilon_o| \ll 1 \qquad \alpha^2 \ll 1$$

Equations (24) are first expanded in powers of ϵ_o and α. Terms up to linear in ϵ_o and up to α^2 are retained in the expansion. See [3] for details:

$$\left.\begin{aligned} U_{load} &\approx PH\epsilon_o - P\alpha^2\tfrac{\pi^2}{4\lambda n} \\ U_{strain} &\approx \alpha^2\tfrac{\pi^4 EI}{(\lambda n)^3} \\ U_{spiral} &\approx \alpha\tfrac{T\pi}{6}\textstyle\sum_{i=1}^{n-1}\left(1-\cos\frac{2\pi i}{n}\right) \\ &\quad + \alpha^2\tfrac{2T}{3\pi R}\textstyle\sum_{i=1}^{n-1}\left(1-\cos\frac{2\pi i}{n}\right)^2 \end{aligned}\right\} (25)$$

Where $I = \iint z^2\,dA$ is the second moment of the area.

The growth properties of U_{strain} and U_{spiral} will be of central importance in considering equilibrium for the small deformation case. Notice in (25) the lowest order term in U_{strain} is a square term in α, whereas, U_{spiral} contains a linear term. Therefore, when α is small, the energy employed in deforming the spiral will dominate the energy employed in deforming the bar.

For the special case when $n = 1$ the dominance of U_{spiral} no longer holds. Notice that

[3] Since we will consider finite deformation from the compressed state, the assumption that arc length doesn't change between these two states may seem implausible. However, a finite element analysis based on more general kinematics [3] verifies the validity of the assumption.

when $n = 1$ the summations appearing in the expression for U_{spiral} vanish. This case corresponds to buckling over a single spiral spacing, which leaves the spiral undeformed.

With these points in mind let us precede with determining the load, P, which will hold the infinitesimally deformed bar in equilibrium. Substituting equations (25) into the potential energy equation (1) yields,

$$\begin{aligned} U \approx\ & PH\epsilon_o - P\alpha^2\tfrac{\pi^2}{4\lambda n} + \alpha^2\tfrac{\pi^4 EI}{(\lambda n)^3} \\ & + \alpha\tfrac{T\pi}{6}\textstyle\sum_{i=1}^{n-1}\left(1-\cos\tfrac{2\pi i}{n}\right) \\ & + \alpha^2\tfrac{2T}{3\pi R}\textstyle\sum_{i=1}^{n-1}\left(1-\cos\tfrac{2\pi i}{n}\right)^2 \end{aligned} \tag{26}$$

Making use of the one-parameter equilibrium equation (17),

$$\begin{aligned} \tfrac{\partial}{\partial\alpha}U \approx\ & -P\alpha\tfrac{\pi^2}{2\lambda n} + \alpha\tfrac{2\pi^4 EI}{(\lambda n)^3} \\ & + \tfrac{T\pi}{6}\textstyle\sum_{i=1}^{n-1}\left(1-\cos\tfrac{2\pi i}{n}\right) \\ & + \alpha\tfrac{4T}{3\pi R}\textstyle\sum_{i=1}^{n-1}\left(1-\cos\tfrac{2\pi i}{n}\right)^2 = 0 \end{aligned}$$

and solving for P gives:

$$\begin{aligned} P =\ & \tfrac{4\pi^2 EI}{(\lambda n)^2} + \tfrac{1}{\alpha}\tfrac{T\lambda n}{3\pi}\textstyle\sum_{i=1}^{n-1}\left(1-\cos\tfrac{2\pi i}{n}\right) \\ & + \tfrac{4T\lambda n}{\pi^3 R}\textstyle\sum_{i=1}^{n-1}\left(1-\cos\tfrac{2\pi i}{n}\right)^2 \end{aligned} \tag{27}$$

The *critical load*, P_{cr} is the minimum value of P in the limit as $\alpha \to 0$ for all possible choices of n,

$$P_{cr} = \min_{n\geq 1}\left(\lim_{\alpha\to 0} P\right).$$

Considering equation (27), notice that it is a sum of positive terms. The first term is the resistance to the axial force due to the strain energy. The second and third terms are the resistance to the axial force generated by the spiral. The second term becomes large for small values of α. So for small values of the buckling amplitude, the force generated by the spiral will be large. However, in the case that the buckling mode is over a single spacing, $n = 1$, the summations vanish— the spiral is undisplaced by the buckle.

As a result the single spacing buckling mode will always furnish the critical load.

$$P_{cr} = \frac{4\pi^2 EI}{\lambda^2} \tag{28}$$

This is the Euler buckling load for fixed–fixed end conditions with a length of one spiral spacing.

In addition, equation (27) suggests that for larger values of α, this may not be the case. As α becomes finite, the second term may no longer dominate and other buckling modes may be possible. However, to consider this we can no longer make assumptions about the magnitude of α. This will motivate us to consider equilibrium in finite deformation.

Single–Spacing Mode for Plastic Case

Before moving onto the finite deformation case, briefly consider the bar deforming as described above but in the plastic range of material response. In the famous experimental observations of F.R. Shanely [7], he observed that during the initial stages of inelastic buckling, all fibers of the bar load monotonically in compression (no strain reversal). This allows us to employ the Deformation Theory of Plasticity.

To allow our previous results (25), (26), (27), (28) to consider the plastic small deformation case, we need only replace the elastic strain energy, U_{strain} with the area under the plastic stress–strain diagram W_{plas}; Figure 8. Note that the slope of the plastic stress–strain diagram is bounded above by E. Consider our result in (27). Only the first term is due to U_{strain}. When the plastic response is considered this term cannot be any greater than the result from elasticity. The other two terms are independent of U_{strain} so they remain the same.

So, for the plastic case the result remains intact. The spiral terms preclude buckling for all modes except $n = 1$. And for the case of $n = 1$ the summations vanish and we have a critical load that is bounded above by the elastic case. Therefore, the conclusion is drawn that even for the plastic case, the buckling begins over a single spacing.

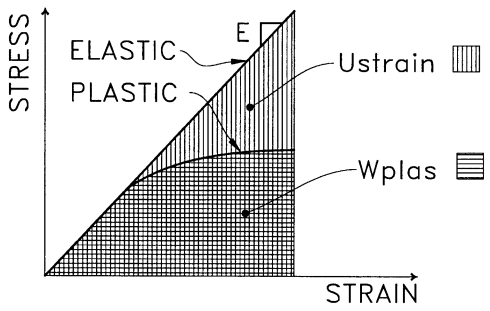

Figure 8: Mechanical work and elastic strain energy

Finite Deformation Buckling

We now return to the linear elastic material and proceed to consider finite deformation. In the last section, it was shown that for an initially straight bar, the buckle will always begin over one spiral spacing. In this section it will be shown that as the buckle grows in amplitude, it can jump over more spacings.

Kinematic Assumption – Near Inextensibility

Although no assumption is made about the size of the amplitude, α, we can still make an assumption about the size of ϵ_o. Recall that ϵ_o is the strain in the bar when it is straight and loaded with axial load P. Since the bar is slender, $\epsilon_o \ll 1$.

Reexamine equations (24) where the terms in the potential energy equation are functions of ϵ_o, α and n. Now we expand in ϵ_o, keeping only linear terms. Equations (24) become, [4]

$$\begin{aligned} U_{load} &\approx -P\left[\Delta\tilde{H}(\epsilon_o,\alpha,n)\right]_{\epsilon_o=0} \\ &\quad - P\,\epsilon_o\left[\tfrac{\partial}{\partial\epsilon_o}\Delta\tilde{H}(\epsilon_o,\alpha,n)\right]_{\epsilon_o=0} \\ U_{strain} &\approx \left[\tilde{U}_{strain}(\epsilon_o,\alpha,n)\right]_{\epsilon_o=0} \\ &\quad + \epsilon_o\left[\tfrac{\partial}{\partial\epsilon_o}\tilde{U}_{strain}(\epsilon_o,\alpha,n)\right]_{\epsilon_o=0} \\ U_{spiral} &= \tilde{U}_{spiral}(\alpha,n)\,. \end{aligned}$$

Substituting $\epsilon_o = -\frac{P}{E\,A_{bar}}$,

$$\begin{aligned} U_{load} &\approx -P\left[\Delta\tilde{H}(\epsilon_o,\alpha,n)\right]_{\epsilon_o=0} \\ &\quad + P^2\tfrac{1}{EA_{bar}}\left[\tfrac{\partial}{\partial\epsilon_o}\Delta\tilde{H}(\epsilon_o,\alpha,n)\right]_{\epsilon_o=0} \\ U_{strain} &\approx \left[\tilde{U}_{strain}(\epsilon_o,\alpha,n)\right]_{\epsilon_o=0} \\ &\quad - P\tfrac{1}{EA_{bar}}\left[\tfrac{\partial}{\partial\epsilon_o}\tilde{U}_{strain}(\epsilon_o,\alpha,n)\right]_{\epsilon_o=0} \\ U_{spiral} &= \tilde{U}_{spiral}(\alpha,n)\,. \end{aligned}$$

These energy functions can now be put into the potential energy equation (1),

$$\begin{aligned} U \approx & -P\left[\Delta\tilde{H}(\epsilon_o,\alpha,n)\right]_{\epsilon_o=0} \\ & + P^2\tfrac{1}{EA_{bar}}\left[\tfrac{\partial}{\partial\epsilon_o}\Delta\tilde{H}(\epsilon_o,\alpha,n)\right]_{\epsilon_o=0} \\ & + \left[\tilde{U}_{strain}(\epsilon_o,\alpha,n)\right]_{\epsilon_o=0} \\ & - P\tfrac{1}{EA_{bar}}\left[\tfrac{\partial}{\partial\epsilon_o}\tilde{U}_{strain}(\epsilon_o,\alpha,n)\right]_{\epsilon_o=0} \\ & + \tilde{U}_{spiral}(\alpha,n)\,. \end{aligned}$$

Again making use of the one-parameter equi-

[4] $\tilde{U}_{spiral}(\alpha,n)$ is unaffected by the expansion since it is not a function of ϵ_o

librium equation (17),

$$\begin{aligned}\frac{\partial}{\partial\alpha}U \approx P^2 \frac{1}{EA_{bar}} \frac{\partial}{\partial\alpha}\left[\frac{\partial}{\partial\epsilon_o}\Delta\tilde{H}(\epsilon_o,\alpha,n)\right]_{\epsilon_o=0} \\ - P \frac{\partial}{\partial\alpha}\left[\Delta\tilde{H}(\epsilon_o,\alpha,n)\right]_{\epsilon_o=0} \\ - P \frac{1}{EA_{bar}} \frac{\partial}{\partial\alpha}\left[\frac{\partial}{\partial\epsilon_o}\tilde{U}_{strain}(\epsilon_o,\alpha,n)\right]_{\epsilon_o=0} \\ + \frac{\partial}{\partial\alpha}\left[\tilde{U}_{strain}(\epsilon_o,\alpha,n)\right]_{\epsilon_o=0} \\ + \frac{\partial}{\partial\alpha}\tilde{U}_{spiral}(\alpha,n) \;=\; 0 .\end{aligned} \tag{29}$$

Equation (29) is quadratic in P. In the range of deformation we are concerned with it has only one positive root, [5]

$$P = \frac{-B(\alpha,n) + \sqrt{B(\alpha,n)^2 + 4\,A(\alpha,n)\,C(\alpha,n)}}{2\,A(\alpha,n)} \tag{30}$$

Where:

$$A(\alpha,n) = -\frac{1}{EA_{bar}} \frac{\partial}{\partial\alpha}\left[\frac{\partial}{\partial\epsilon_o}\Delta\tilde{H}(\epsilon_o,\alpha,n)\right]_{\epsilon_o=0}$$

$$\begin{aligned}B(\alpha,n) = \;& \frac{\partial}{\partial\alpha}\left[\Delta\tilde{H}(\epsilon_o,\alpha,n)\right]_{\epsilon_o=0} \\ & + \frac{1}{EA_{bar}} \frac{\partial}{\partial\alpha}\left[\frac{\partial}{\partial\epsilon_o}\tilde{U}_{strain}(\epsilon_o,\alpha,n)\right]_{\epsilon_o=0}\end{aligned}$$

$$\begin{aligned}C(\alpha,n) = \;& \frac{\partial}{\partial\alpha}\left[\tilde{U}_{strain}(\epsilon_o,\alpha,n)\right]_{\epsilon_o=0} \\ & + \frac{\partial}{\partial\alpha}\tilde{U}_{spiral}(\alpha,n)\end{aligned}$$

Force Displacement Curves

For any value of α and n the terms $A(\alpha,n)$, $B(\alpha,n)$ and $C(\alpha,n)$ can be computed numerically. Therefore, for any amplitude and buckling length, Equation(30) computes the axial load, P, that maintains equilibrium for the system. Once we have determined P and, thus ϵ_o (recall $\epsilon_o = -\frac{P}{E\,A_{bar}}$), we can evaluate ΔH by substituting the assumed deformations (22) and (19) into (3). This procedure was carried out for a system with the parameters shown in Table 1. A plot of P vs. ΔH is shown in Figure 9. Each curve represents the locus of solutions for a buckling length, n. The solid line through the origin represents the straight, compressed solution. The axes are normalized with the critical buckling load, P_{crit}, given by (28) and the shortening of the model compressed under critical load, $\Delta H_{crit} = \frac{P_{crit}\,H}{E\,A_{bar}}$. ($H$ is the length of the model.)

The plots reveal a snap buckling behavior [2]. Notice that as we start to compress the bar, the solution will move along the straight solution until it approaches the critical load.

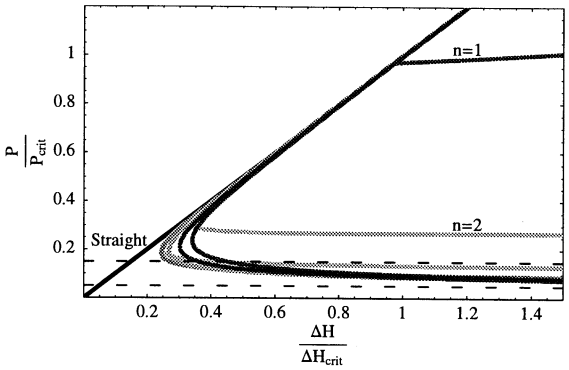

(a) Full view

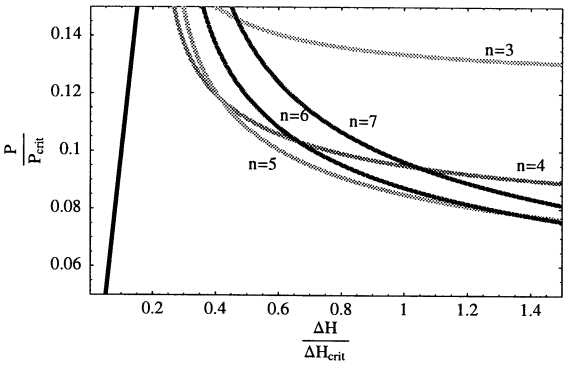

(b) Blow–up of dashed region

Figure 9: Force–displacement curves

[5] It is shown in [3] that the functions $A(\alpha,n)$, $B(\alpha,n)$ and $C(\alpha,n)$ are strictly positive functions when $\alpha < \frac{1}{7}\lambda n$. So we can be sure that there is only one positive root to the quadratic as long as the buckling amplitude is less than one-seventh of the buckling length.

Parameter		*Value*	
Bar Height,	H	10	inches
Bar Diameter,	d_{bar}	0.1	in
Spiral Spacing,	λ	1.25	in
Spiral Diameter,	d_{spir}	0.025	in
Column Radius,	R_0	12	inches
Elastic Modulus,	E	$29\,10^6$	psi
Spiral Yield Force,	T	150	lbs

Table 1: Model parameters

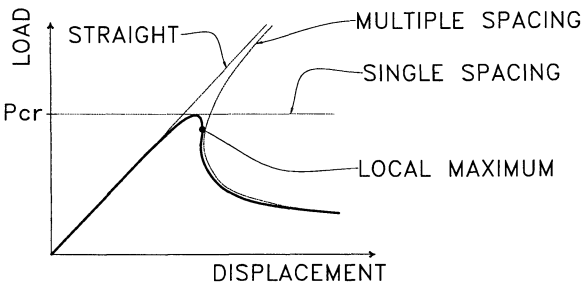

Figure 10: Snap buckling phenomenon

Then the bar will begin to buckle over one spacing. Shortly after beginning to buckle, the solution encounters a local maximum for displacement, ΔH; see Figure 10. As ΔH is increased further snapping occurs because no nearby equilibrium state can be found. The solution snaps to the multiple spacing mode that has the smallest corresponding value for the axial load. Figure 9 reveals that buckling modes $n = 4$ to $n = 6$ become favorable. This transition causes a dramatic decrease in the axial load in the bar.

Finite Element Analysis

In this section, the deformation is no longer assumed to be sinusoidal. Instead we allow the deformation to have a more general form. Previously the equilibrium was determined by varying α, now it is determined by finitely many degrees of freedom. Equilibrium states are solved using a straight–forward non-linear finite element procedure. Because of the presence of second order derivatives, Hermitian interpolation was used on both $u(s)$ and $w(s)$. Contact with the core was treated using a one–way elastic foundation. As before, the material of the longitudinal bar is linear elastic. Only the results of the finite element analysis are presented here. See [3] for a full account of the finite element formulation.

Simulated Test Procedure and Results

A computer simulation of the bar buckling was performed. In order to force the bar to buckle the top of the bar was incrementally displaced downwards. The prescribed axial displacement will be denoted $\overline{\Delta H}$. This is similar to a "displacement controlled" test that would be performed in a laboratory. By prescribing the displacement, we can be assured that a solution exists for each step. On the other hand, if the procedure was to increment the end load, P, we would be unable to solve for equilibrium points on decreasing portions of the force-displacement curve.

In order to keep the bar from remaining straight a small *perturbation force* is applied transversely at midspan of the bar. The magnitude of the perturbation force was small $\approx 10^{-6} P_{crit}$. Using symmetry, only half of the bar was modeled, this constrained the bar to buckle over an odd number of spacings. The model of half of the bar was discretized into 8 elements.

The "test specimen" had the same parameters as were used to generate the force–displacement curve in the previous section. Figure 11 shows the displaced shape of the model at several levels of axial displacement.

No Axial Displacement

Figure 11(a) shows the the bar under the action of the perturbation force alone. The transverse displacement is negligible with a maximum of about 10^{-6} inches.

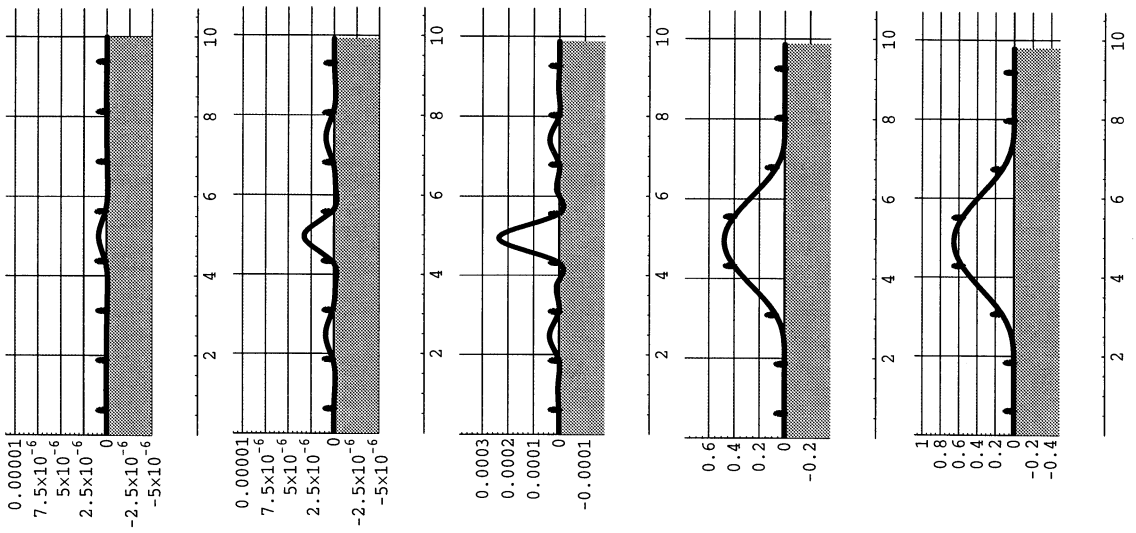

$\Delta H = 0$ (a) $0.5\,\Delta H_{crit}$ (b) $0.75\,\Delta H_{crit}$ (c) $0.8\,\Delta H_{crit}$ (d) $1.3\,\Delta H_{crit}$ (e)

Figure 11: Displaced shape from finite element analysis

Before The Onset of Buckling

As the top of the bar is moved downward the transverse displacement increases gradually, at first. When the axial displacement reaches 0.5 ΔH_{crit}, see Figure 11(b), the transverse displacement has only reached a maximum of $\approx 3 \cdot 10^{-6}$ inches.

The Onset of Buckling - Single Spacing Mode

At 0.75 ΔH_{crit} the bar has buckled over a single spacing; see Figure 11(c). The transverse displacement has increased 100 times to $\approx 3 \cdot 10^{-4}$ inches. The bar buckles before ΔH_{crit} because of differences between the assumed deformed shape and the shape that exhibits itself here and also due to the perturbation force. Observe that the buckling length is greater than one spiral spacing because of penetration of the bar into the core. Recall, the assumed deformation of the last section forced the buckling length to be a whole number of spacings.

Transition to 5-Spacing Mode

When the axial displacement is incremented slightly more to 0.8 ΔH_{crit} the buckling mode jumps to the 5 spacing mode; see Figure 11(d). The transverse displacement increases over one thousand times to ≈ 0.5 inches. Meanwhile, the bar has attained a shape and buckling length very similar to that considered by the assumed deformation of the prior sections.

Bar Remains in 5-Spacing Mode

As the axial displacement is incremented further the buckling mode remains at 5 spacings and the transverse displacement increases gradually; see Figure 11(e). Even though the axial displacement has increased from 0.8 ΔH_{crit} to 1.3 ΔH_{crit} the lateral displacement has only increased to ≈ 0.65 inches.

Force vs. Displacement

Figure 12 shows a plot of axial reaction, P, versus prescribed axial displacement for the test just discussed. The data from the finite element analysis is plotted as points over the force

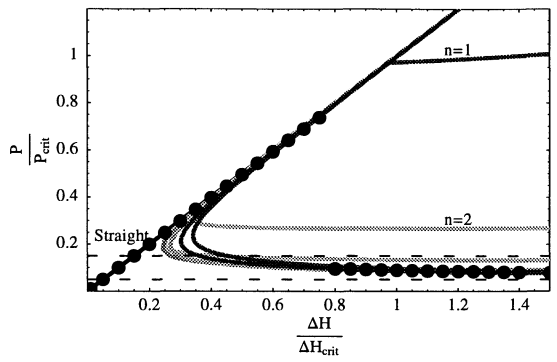

(a) Full view

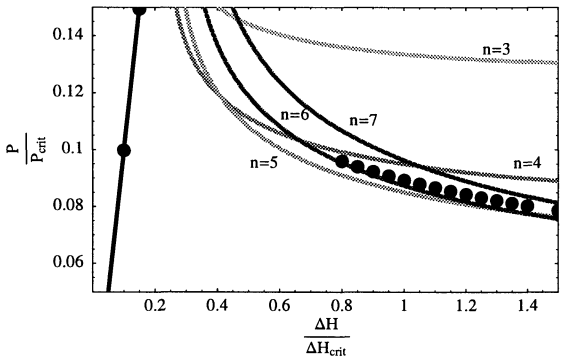

(b) Blow–up of dashed region

Figure 12: Axial reaction, P vs. prescribed axial displacement $\overline{\Delta H}$

versus displacement curves generated analytically. The plot reveals good agreement with the analytical result, even for displacements that are quite large.

We see that for small loadings the solution travels along the solution for the straight bar. When the bar buckles, the interval of ΔH where the bar buckles in the single spacing mode is very short so it does not appear demonstratively on the plot. Then the solution makes the transition to a multiple–spacing mode causing the axial load to drop sharply. The remainder of the test is spent in the multiple–spacing mode. Inside of the multiple spacing regime, the axial load behaves in a stable manner for a large range of axial displacements.

Conclusions

Column reinforcement in the laboratory and field is observed to buckle over multiple spacings. Present models are unable to adequately explain this behavior analytically. The model presented in this paper allows consideration of finite deformation and the prestressing of the confining spiral. This model has significant advantages over other models for explaining observable buckling modes since it allows the phenomenon to be modeled accurately to a level of deformation that is visible.

Analytical results of the model reveal that an initially straight bar must initiate buckling over a single spacing for both the elastic and plastic case.

For the finite deformation case, only elastic models for the buckling bar are considered. We have demonstrated analytically and computationally that after the single-spacing buckling grows, it "snaps" to a multiple–spacing buckling mode similar to that observed in reinforcing bars. After the buckled bar has snapped into the longer mode its ability to support axial loads is diminished.

These results throw into question the validity of models which only consider small deformations from the straight configuration. Models of that type are only capable of predicting the onset of buckling. Any transition of buckling modes that may occur subsequent to the onset of buckling would occur beyond their domain of applicability.

Since the work presented considers only the finite deformation behavior of initially straight bars which buckle elastically, the explanation it presents for the real system is promising but far from complete. In order to truly understand this phenomenon, a more representative constitutive law should be used. In addition, we must begin to investigate the effect of the initially out–of–straight condition that is present in real reinforcing bars.

References

[1] Bresler, B., and Gilbert, P. H. (1961). "Tie requirements for reinforced concrete columns." *ACI J.*, 58(26), 555-570.

[2] Budiansky, B. (1974). "Theory of buckling and post–buckling behavior of elastic structures." *Adv. Apl. Mech.* 14, 1–65.

[3] Falk, W. M. (1999). "An elastic explanation for the observed buckling mode of reinforcing bars in concrete." Master's thesis, Department of Civil Engineering, University of California, Berkeley. Technical Report UCB/SEMM-1999/08.

[4] Mau, S.T. and El-Mabsout, M. (1989). "Inelastic buckling of reinforcing bars." *J. Engrg. Mech.*, ASCE, 115(1), 1-17.

[5] Pantazopoulou, S. J. (1998). "Detailing for reinforcement stability in RC members." *J. Struct. Engrg.*, ASCE, 124(6), 623-632.

[6] Papia, M., Russo, G., and Zingone, G. (1988). "Instability of longitudinal bars in RC columns." *J. Struct. Engrg.*, ASCE, 114(2), 445-461.

[7] Shanely, F. R. (1947). "Inelastic column theory." *J. Aero. Sci.* 14, 261–268.

[8] Timoshenko, S. P. (1936). *Theory of elastic stability*, 1st Ed., p. 109, McGraw-Hill, New York.

[9] Watson, S., Zahn, F. A., and Park, R. (1992). "Confining reinforcement for concrete columns." *J. Struct. Engrg.*, ASCE, 120(6), 1798-1824.

[10] Washizu, K. (1968). *Variational methods in elasticity and plasticity.* 1st Ed. Pergamon Press, Oxford.